Shape optimization of reduced beam section under cyclic loads

M. Ohsaki[1] *, H. Tagawa[2] and P. Pan[3]

[1]*Department of Architecture and Architectural Engineering, Kyoto University, Kyoto-Daigaku Katsura, Nishikyo, Kyoto, 615-8540, Japan,*
[2]*Department of Environmental Engineering and Architecture, Nagoya University, Furo-cho, Chikusa, Nagoya 464-8603, Japan,*
[3]*Department of Civil Engineering, Tsinghua University, Beijing 100084, P.R. China*

Abstract

Optimal shapes are found for reduced beam section of a cantilever H-beam subjected to forced cyclic displacement at the free end. The beam is discretized to finite elements, and a commercial software package called ABAQUS is used for elastoplastic analysis. The numerical results are first compared with experimental results to verify the accuracy. The objective function to be maximized is the dissipated energy throughout the loading history. The constraint is given for the maximum equivalent plastic strain at the welded section. Global optimal solutions are searched by a heuristic approach called simulated annealing, which is successfully combined with ABAQUS. It is shown that the energy dissipation capacity is significantly improved by optimizing the flange shape.

Key words: Shape optimization; H-beam; Reduced beam section; Plastic energy dissipation; Simulated annealing

* Corresponding author. Tel: +81-75-383-2901 Fax: +81-75-383-2972.
  Email addresses: `ohsaki@archi.kyoto-u.ac.jp` (M. Ohsaki[1]),
`tagawa@genv.nagoya-u.ac.jp` (H. Tagawa[2]), `panpeng@mail.tsinghua.edu.cn` (P. Pan[3]).

1 Introduction

Most of the optimization approaches for steel frames are concerned with stiffness design of beams and columns, where the cross-sectional properties are considered as design variables. Elastic responses such as stresses and displacements under static loads are usually considered as design constraints. However, it is possible to optimize the cross-sectional properties of members to maximize plastic energy dissipation under seismic excitations [1].

On the other hand, in the fields of mechanical engineering and aeronautical engineering, shapes of structural components or parts, such as airfoil wing of aircraft and engine mount of automobile, are optimized using finite element discretization [2,3]. However, in these studies, only elastic responses are considered.

In the 1994 Northridge earthquake, we experienced serious damage to steel moment-resisting frames mainly due to brittle fracture near the beam-to-column flange groove welds. In response to such damage, a wide variety of connection concepts have been developed and revisited [4,5]. Among them, the Reduced Beam Section (RBS) connection attained much popularity, particularly in the West Coast of U.S. A significant amount of research has already been conducted including the tests on RBS connections with constant cuts and tapered cuts prior to Northridge earthquake [6,7], and the tests and analyses on RBS connections including circular cut after the earthquake [8–12]. Shen *et al.* [13] investigated the seismic performance of a frame with RBS. Kassegne [14] developed a finite element model for a beam with RBS.

In an RBS moment connection, portions of the beam flanges are selectively trimmed to force a plastic hinge to be located within the reduced section, and thereby reduce the likelihood of fracture occurring at the beam-to-column flange groove welds. Optimizing the shape of the RBS cut can increase the energy dissipation capacity of the connection, and further minimize the likelihood of fracture in the flange by realizing widely distributed plastification with less maximum plastic strain. According to a summary of the tests before 2000 [15], the circular cut tends to minimize stress concentration compared with the constant cut or tapered cut, both of which have reentrant corners. However, most of the investigations on optimization of cutout shape up to date are based on predetermined shapes [16]. Pan *et al.* [17] investigated optimal flange shape under monotonic loads. However, for application to seismic design, cyclic loads should be considered.

Optimization of elastoplastic structures has been extensively investigated in 1990s including sensitivity analysis of path-dependent problems [18–21]. Approximation methods such as response surface method are currently applied to an elastoplastic optimization problem, because it usually has multiple local optima and application of gradient-based approach is not desirable.

Heuristic approaches have been developed to obtain approximate optimal solutions within reasonable computational time, although there is no theoretical proof of convergence [22]. The most popular approach is the genetic algorithm, which is a multi-point method that has many solutions at each iterative step called generation. Since computational cost for function evaluation is not small for structural optimization problems, a multi-point strategy may not be appropriate especially for structures with large degrees of freedom under path-dependent constraints.

Simulated Annealing (SA) is categorized as a single-point search heuristic approach

that is based on local searches and improves ability of finding global optimal solution by allowing the move to a non-improving solution with a specified probability [23]. SA has been successfully applied to many structural optimization problems [24, 25], and is applicable to both problems with continuous and discrete variables.

Shape optimization of continuum structures has been investigated mainly for elastic problems. It is well known that the optimal boundary shape may not be smooth due to numerical instability if the locations of all the boundary nodes of the finite elements are considered as independent variables [26]. Therefore, smoothing by Bézier curves or B-spline curves has been presented using the techniques of computer-aided geometrical design [27], which are widely used for shape optimization of curved surfaces [28].

In this paper, we present a method of optimizing shapes of reduced beam section based on SA, which is successfully combined with a commercial finite element analysis software package called ABAQUS [29]. The objective function to be maximized is the dissipated energy under cyclic static load. Constraint is given for the maximum equivalent plastic strain along the welded section at the beam-to-column connection. It is shown in the numerical examples that the energy dissipation capacity under cyclic loading can be significantly improved by optimizing the shape of the flange.

2   Optimization problem and flange model

Consider a cantilever beam discretized to finite elements, which represents a half of a beam in a frame. The free end corresponds to the inflection point at the mid-span of the beam. Optimal flange shapes are to be found under cyclic static loading condition defined by forced displacement at the free end.

The shape of flange is defined by a cubic spline curve, and the design variables are the locations of the control points. Let $\boldsymbol{y}$ denote the vector consisting of the variable coordinates of the control points. The upper and lower bounds for $\boldsymbol{y}$ are denoted by $\boldsymbol{y}^{\mathrm{U}}$ and $\boldsymbol{y}^{\mathrm{L}}$, respectively. In the following, a component of a vector is indicated by subscript; e.g., $\boldsymbol{y} = (y_1, \ldots, y_m)$, where m is the number of design variables.

The objective function is the dissipated energy throughout the loading history, which is denoted by $E(\boldsymbol{y})$ as a function of $\boldsymbol{y}$. Since the loading is given as a forced displacement, an unfavorable local plastification can be avoided by maximizing $E(\boldsymbol{y})$. The upper bound $\bar{\varepsilon}^{\mathrm{p}}$ is given for the maximum equivalent plastic strain ε^{p} among the elements along the fixed end to prevent fracture at the beam-to-column flange groove welds. Hence, the optimization problem is formulated as

$$\text{maximize} \quad E(\boldsymbol{y}) \tag{1}$$
$$\text{subject to} \quad \varepsilon^{\mathrm{p}}(\boldsymbol{y}) \leq \bar{\varepsilon}^{\mathrm{p}} \tag{2}$$
$$y_i^{\mathrm{L}} \leq y_i \leq y_i^{\mathrm{U}}, \quad (i = 1, \ldots, m) \tag{3}$$

In the numerical example, optimal flange shapes are to be found for a cantilever beam with a cross-section of H-300×150×6.5×9. The length L of the cantilever beam is 1218 mm. Hence, the span-height ratio of the beam to be simulated is $1218 \times 2/300 = 8.12$.

Fig. 1 shows the normal flange shape. The flange width is to be varied at the 450 mm
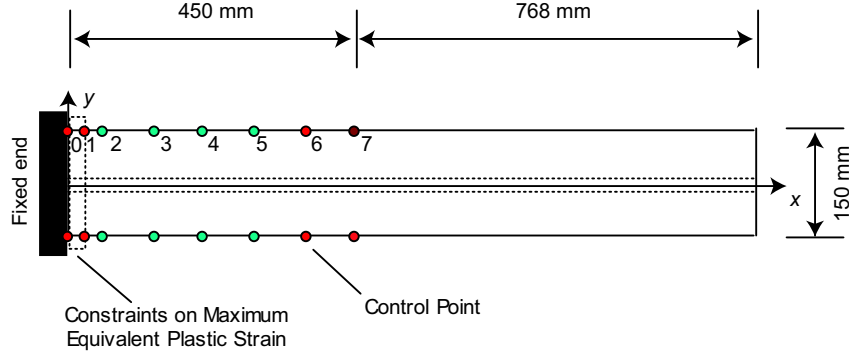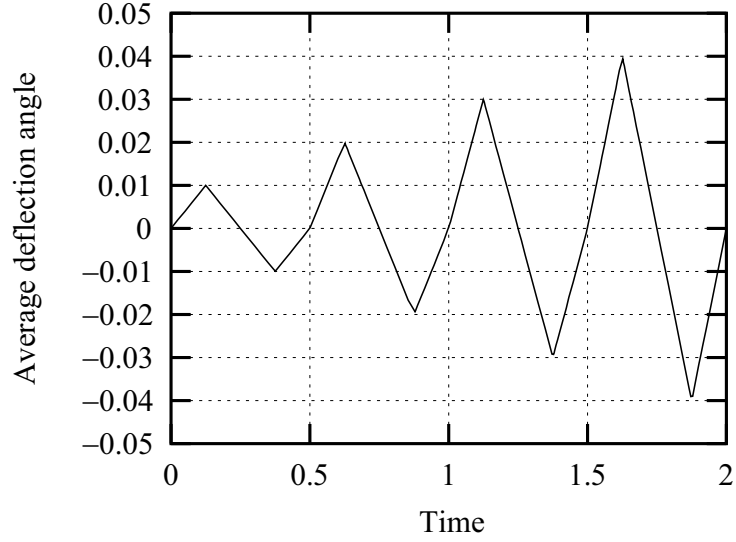
3

Fig. 1. Normal flange shape.

Fig. 2. Loading history.

region from the welded section. The control points for the cubic spline curve are given as shown in Fig. 1. The (x, y)-coordinates (mm) of the points 0, 1, 2 and 7 are fixed at $(0.0, 75.0)$, $(25.0, 75.0)$, $(50.0, 75.0)$ and $(450.0, 75.0)$, respectively. The points 3–6 can move only in y-direction, and their x-coordinates are fixed at 130, 210, 290 and 370 (mm), respectively. Therefore, the number of design variables is 4 considering the symmetry condition with respect to the x-axis. The upper and lower bounds of the variables are 75.0 mm and 25.0 mm, respectively; i.e., only reduction is allowed for the flange width at the control point. However, the width between the control points may slightly increase as a result of cubic interpolation.

The history of the average deflection angle θ under cyclic forced displacement at the free end is specified as shown in Fig. 2. The elastic modulus is 2.05×10^5 N/mm^2 and Poisson's ratio is 0.3. Elastoplastic analysis is carried out by ABAQUS Ver. 6.5.3 [29]. S4R, which is a 4-node quadrilateral thick shell element with reduced integration and a large-strain formulation, is used, and a combined nonlinear kinematic-isotropic hardening with Ziegler's rule is adopted. The total numbers of elements and degrees of freedom of displacements are 1200 and 7650, respectively, for the RBS models for optimization.

4

Table 1. Material properties of the beam and columns.

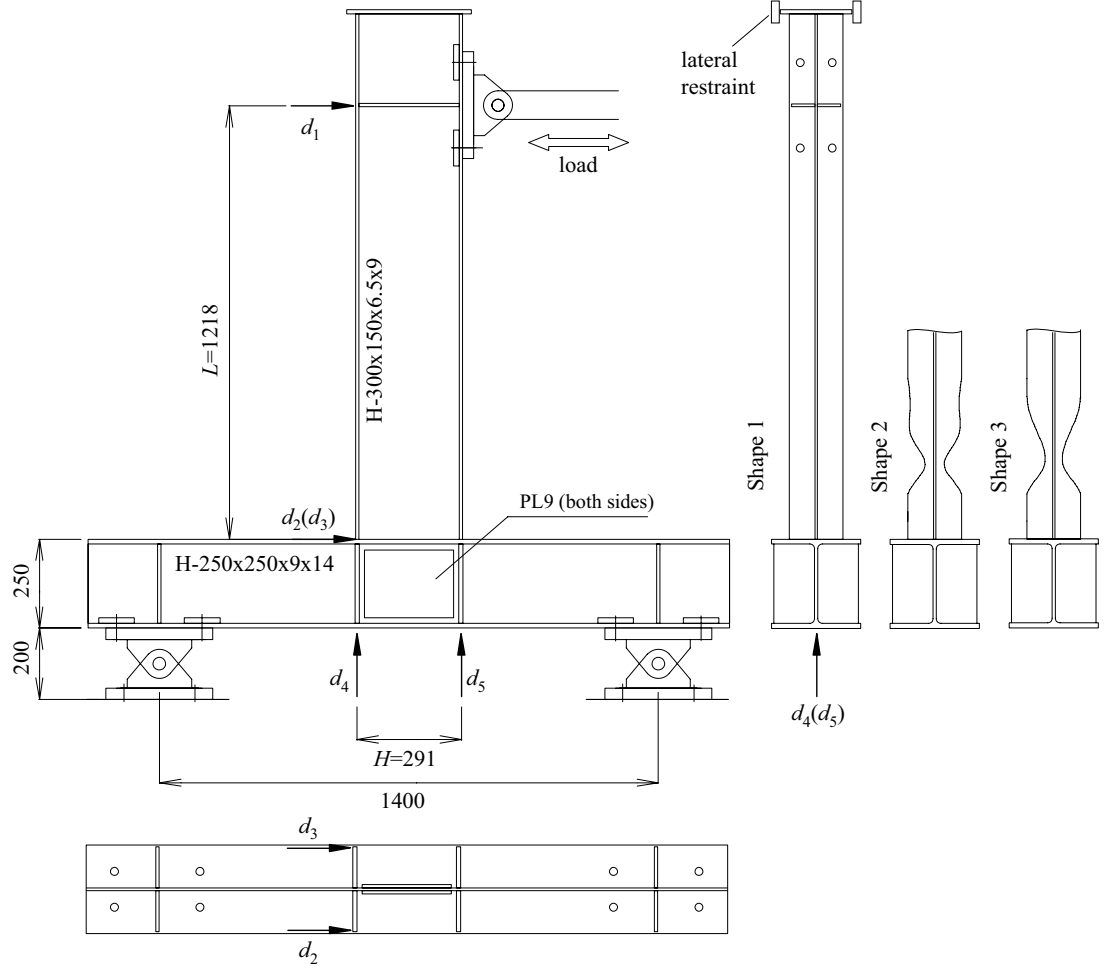|		yield stress (N/mm^2)	tensile strength (N/mm^2)	maximum elongation (%)
beam	flange	365	467	25.0
H-300×150×6.5×9	web	393	479	19.0
column	flange	276	433	32.5
H-250×250×9×14	web	298	443	30.5

Fig. 3. Geometry of the specimen and the locations of the loading and measuring devices.

3 Verification of finite-element analysis

Before carrying out numerical optimization, the results of finite element analysis is compared with experimental results for verification of accuracy of the finite element model. Fig. 3 shows the geometry of the specimen as well as the locations of the loading and measuring devices. The vertical beam, for which the flange shape is to be varied, is supported by a pair of horizontal columns, which has the cross-section of H-250×250×9×14. The measured thicknesses of the flange and web of the beam are 8.8 mm and 6.35 mm, respectively. The horizontal columns are pin-supported at the two ends, and the forced
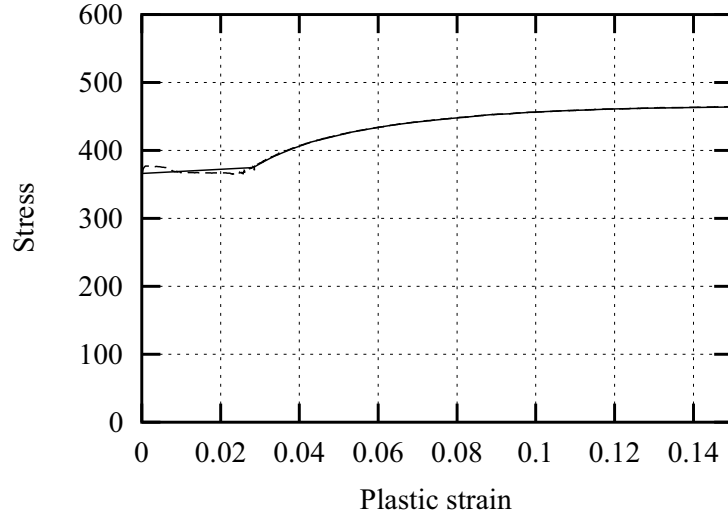
(a) flange
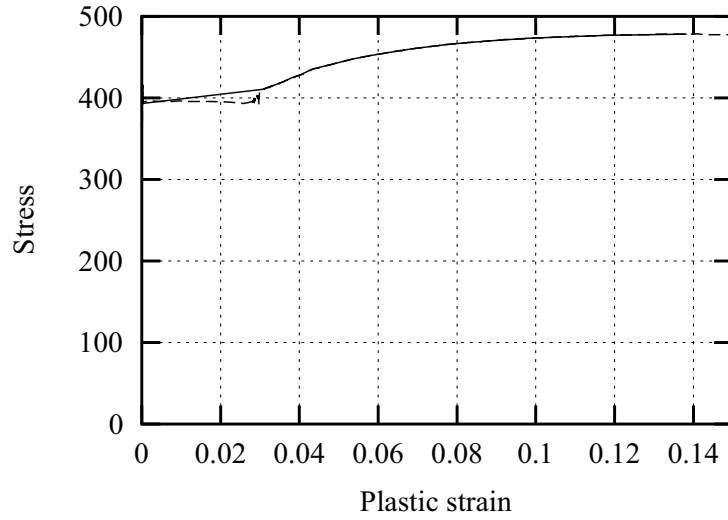
(b) web

Fig. 4. Material properties of flange and web; solid line: approximate relation, dotted line: experimental result.

displacement is applied at the top of the vertical beam using a 1 MN capacity hydraulic jack. Out-of-plane movement is prevented by lateral restraints at the endplate close to the loading point. The displacements $d_1, \ldots, d_5$ are measured as indicated in the figure. The material properties of beam and columns are listed in Table 1, and the results of monotonic coupon test for the flange and web of the beam are shown in Figs. 4(a) and (b), respectively. The dotted and solid lines in Figs. 4(a) and (b) show the relations before and after interpolation near the yield point. The interpolated approximate data are assigned to ABAQUS, which automatically identifies the nonlinear hardening parameters. Note that the data have been interpolated so that the stress is an increasing function of the plastic strain, because otherwise parameter identification by ABAQUS failed.

6

Table 2. (x, y)-coordinates (mm) of control points of the experimental models.

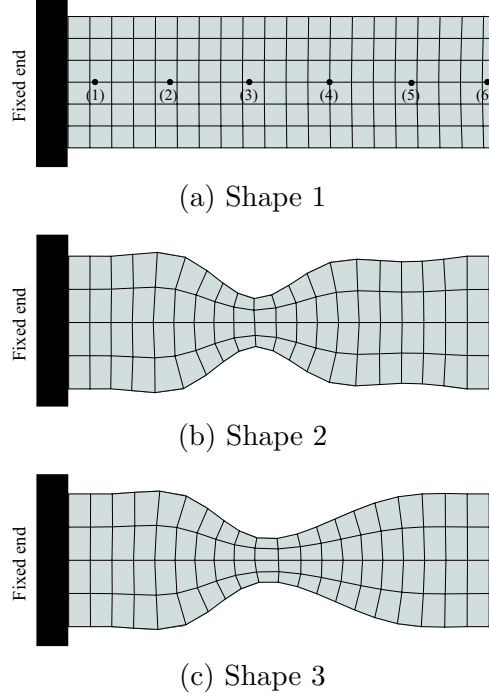| Point	3	4	5	6
Shape 1	(130.0,75.0)	(210.0,75.0)	(290.0,75.0)	(370.0,75.0)
Shape 2	(130.0,75.0)	(210.0,57.0)	(290.0,74.8)	(370.0,74.8)
Shape 3	(130.0,62.3)	(210.0,47.7)	(290.0,70.8)	(370.0,74.9)

(a) Shape 1

(b) Shape 2

(c) Shape 3

Fig. 5. Finite element models for verification of numerical results, and location of strain gages.

In the experiment, the rotation θ_J of the joint is canceled to compute θ as

$$\theta = \frac{d_1 - (d_2 + d_3)/2}{L} - \theta_\mathrm{J} \tag{4}$$

where θ_J is given as

$$\theta_\mathrm{J} = \frac{d_4 - d_5}{H} \tag{5}$$

with $H = 291$ mm as indicated in Fig. 3.

The locations of the control points 3–6 of the three specimens are shown in Table 2, and the finite element models for verification of numerical results are shown in Fig. 5(a)–(c). The width exceeding the normal value 150 mm due to cubic interpolation is truncated at 150 mm. The relations between the average deflection angle and the applied load by the experiment are plotted in dashed lines in Fig. 6(a)–(c).

The relations between the average deflection angle and the applied load by numerical analysis are plotted in solid lines in Fig. 6(a)–(c). Good agreement can be observed between experimental and numerical results for the overall relations between the load and the average deflection angle.
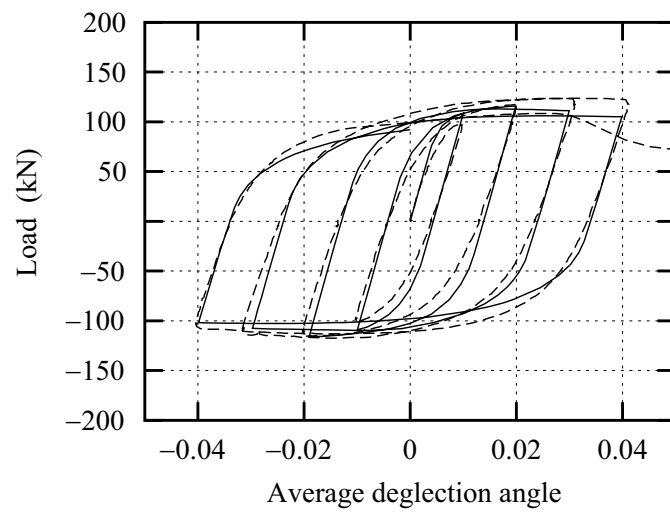
The strains in the compressive flange in x-direction at the load level 20, 40, 60, 80 and 95 (kN), before the initial peak at $t = 0.125$ in Fig. 2, are plotted in Fig. 7(a)–(c). Note
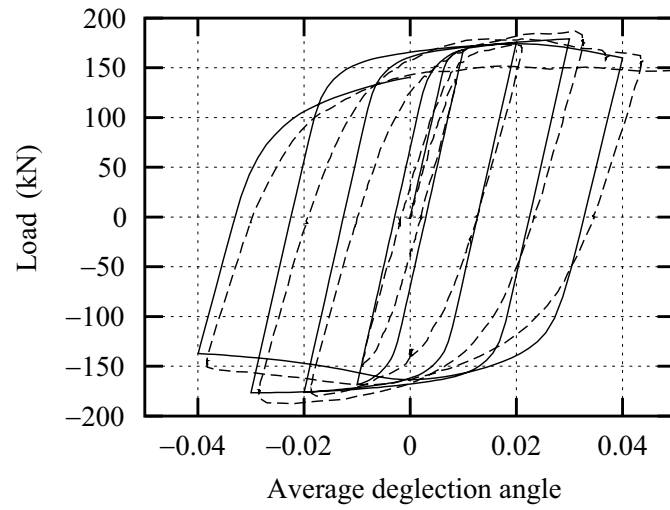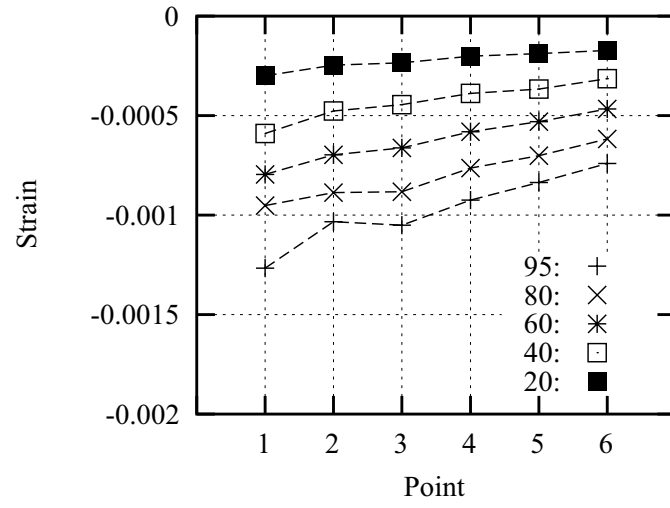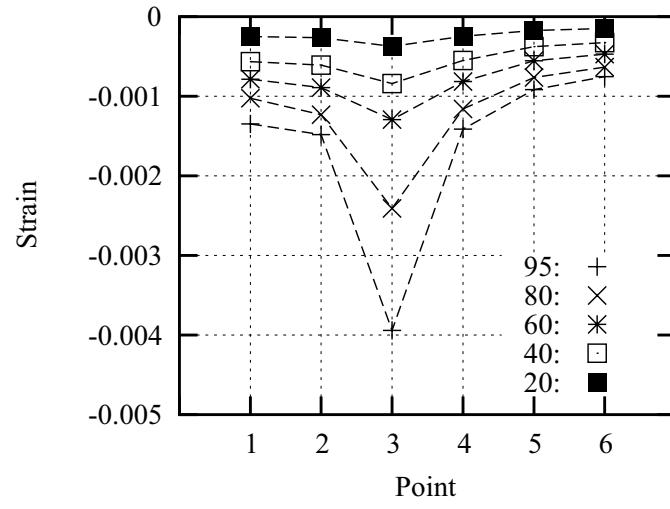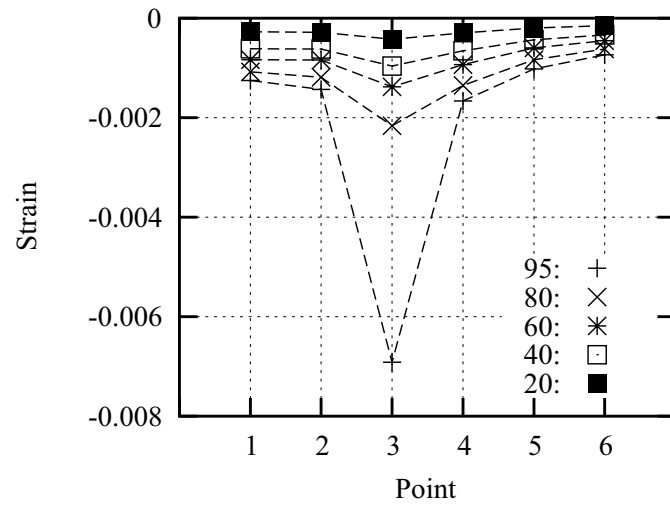
(a) Shape 1
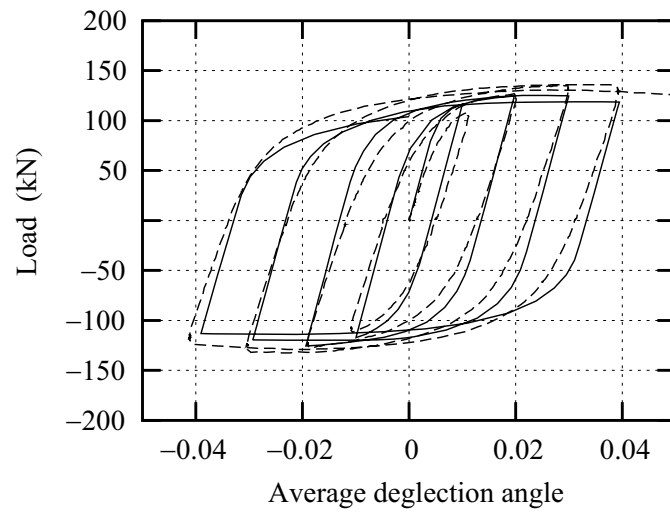
(b) Shape 2

(c) Shape 3

Fig. 6. Load-deflection relation by experiment and numerical analysis.

8

(a) Shape 1

(b) Shape 2

(c) Shape 3

Fig. 7. x-directional strains at points (1)–(6) on the compressive flange.

9

that the load at $t = 0.125$ of Shape 3 is about 98 kN. The strain gages are mounted on the beam flange at the points (1)–(6) indicated in Fig. 5(a). It can be seen that the strains near the fixed end of Shapes 2 and 3 are below yield strain. The largest strain is observed at point (3) in the region of reduced section of Shape 3 that has the smallest width among the three cases.

4 Simulated annealing

SA is an optimization algorithm categorized as a statistical search method. It is based on the local search and prevents convergence to a local optimal solution by allowing the move to a solution that does not improve the objective value. The term *simulated annealing* comes from the fact that it simulates the behavior of the metals in annealing process.

In this paper, the SA for continuous variables by Goffe *et al.* [30] is used. The main feature of this method is that it controls the size of the most promising area defined by the vector $\boldsymbol{s} = (s_1, \ldots, s_m)$ composed of maximum distance for each variable to the neighborhood solutions, which is initially moderately large, and gradually reduced to reach the global optimum. The speed of reduction is controlled by a parameter N_S as described below.

The constraint $\varepsilon^{\mathrm{p}} \leq \bar{\varepsilon}^{\mathrm{p}}$ is incorporated by a penalty function approach. Let $\eta\ (> 0)$ denote the penalty parameter. The objective function is transformed to $\tilde{E}$ as

$$\tilde{E}(\boldsymbol{y}) = E(\boldsymbol{y}) - \eta \max(0, \varepsilon^{\mathrm{p}}(\boldsymbol{y})/\bar{\varepsilon}^{\mathrm{p}} - 1) \tag{6}$$

The algorithm is summarized as follows, where the superscript $(\cdot)^{(k)}$ denotes a value at the kth iteration:

Step 1 Specify the parameters N_S, N_T, μ, η, the scaling parameter c for the temperature, and assign the initial values for $\boldsymbol{s}$ and the temperature parameter T. Note that N_T and μ control the speed of reduction of T. Randomly generate the initial values $y_i^{(0)}$ $(i = 1, \ldots, m)$ of the variables, and set the iteration counter $k = 0$.

Step 2 Choose $i \in \{1, 2, \ldots, m\}$ and generate a random number $r_i \in [0, 1)$ to obtain a neighborhood solution $\boldsymbol{y}^*$ of the current solution $\boldsymbol{y}^{(k)}$ by modifying the ith variable as

$$y_i^* = y_i^{(k)} + (2r_i - 1)s_i \tag{7}$$

If $y_i^* < y_i^{\mathrm{L}}$ or $y_i^* > y_i^{\mathrm{U}}$, assign a randomly selected value for y_i^* satisfying $y_i^{\mathrm{L}} \leq y_i^* \leq y_i^{\mathrm{U}}$. Define $\Delta \tilde{E} = \tilde{E}(\boldsymbol{y}^*) - \tilde{E}(\boldsymbol{y}^{(k)})$. If $\Delta \tilde{E} > 0$, let $\boldsymbol{y}^{(k+1)} = \boldsymbol{y}^*$. Otherwise, accept $\boldsymbol{y}^*$ by the probability P defined as

$$P = \exp\left(\frac{-\Delta \tilde{E}}{cT}\right) \tag{8}$$

Update the counter as $k \leftarrow k + 1$, and carry out this step m times for $i = 1, 2, \ldots, m$.

Step 3 At every mN_S function evaluations, decrease each component of $\boldsymbol{s}$ as described below.

Step 4 If the number of function evaluations at the same temperature level exceeds $mN_\mathrm{T}N_\mathrm{S}$, decrease the temperature parameter as $T \leftarrow \mu T$.

Step 5 Go to Step 2 if the stopping criteria are not satisfied. Otherwise, output the best solution satisfying the constraint, and terminate the process.

The parameter s_i is adjusted as follows so that about 50% of neighborhood solutions are accepted:

Step 3.1 Let N_i^A denote the number of trials accepted for modification of y_i. Let $R_i = N_i^\mathrm{A}/N_\mathrm{S}$ $(i = 1, 2, \ldots, m)$.

Step 3.2 For each $i \in \{1, 2, \ldots, m\}$, multiply s_i by λ_i, which is defined as

$$\lambda_i = \begin{cases} 1 + 2(R_i - 0.6)/0.4 & \text{for } R_i > 0.6 \\ 1/(1 + 2(0.4 - R_i)/0.4) & \text{for } R_i < 0.4 \end{cases} \tag{9}$$

If $s_i > y_i^\mathrm{U} - y_i^\mathrm{L}$, replace s_i by $y_i^\mathrm{U} - y_i^\mathrm{L}$.

The idea is that if T is large relative to $y_i^\mathrm{U} - y_i^\mathrm{L}$, the neighborhood solution for most case will be accepted, forcing s_i to increase. On the other hand, s_i decreases as T is reduced to maintain about 50% acceptance ratio. When T decreases to a small value, the local search can be done in the most promising small area for global optimum.

5   Optimization results

Optimal shapes of reduced beam section are found for a cantilever H-beam subjected to cyclic loading condition defined in Fig. 2. The detailed geometry and material properties have been shown in Sections 2 and 3.

The parameters for SA are $N_\mathrm{T} = 2$, $N_\mathrm{S} = 20$, $\mu = 0.85$, $c = 100$ and the initial temperature is 1.0. The value of the penalty parameter η is set so that the magnitude of the penalty term in (6) is about 10-times as large as the possible value of E at the initial temperature. The initial value of s_i is 10.0. These parameters have been adjusted by several trial runs. If the search region becomes small too rapidly, then the value of N_S should be increased. If too many non-improving solutions are accepted, the value of N_T should be decreased. The stopping criterion is given such that the improvement of $\tilde{E}$ is less than the small value 0.1 within consecutive four steps of decreasing the temperature. The ABAQUS analysis is iteratively called from the SA algorithm. See Appendix for details. A personal workstation with AMD Opteron 2.6 GHz (2 CPUs), 2GB RAM is used for the computation.

Response of the beam with normal flange (referred to as Case 0 hereafter) is first computed to determine the upper-bound values for the optimization problem. Let $\bar{\varepsilon}^\mathrm{p0} = 0.47342$ denote the maximum equivalent plastic strain among the elements along the fixed end. We generate optimal shapes for the two cases as

- Case 1: $\bar{\varepsilon}^\mathrm{p} = \bar{\varepsilon}^\mathrm{p0}/10 = 0.047342$
- Case 2: $\bar{\varepsilon}^\mathrm{p} = \bar{\varepsilon}^\mathrm{p0}/50 = 0.0094683$

11

(a) Case 1 $(\bar{\varepsilon}^{\mathrm{p}} = 0.047342)$

(b) Case 2 $(\bar{\varepsilon}^{\mathrm{p}} = 0.0094683)$
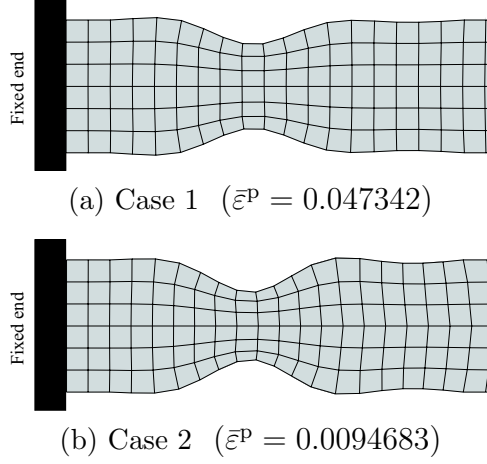
Fig. 8. Optimal shapes.

Table 3. y-coordinate (mm) of the control points of the normal and optimal shapes.

	y_3	y_4	y_5	y_6
Case 0	75.0	75.0	75.0	75.0
Case 1	74.528	47.150	71.012	72.681
Case 2	70.766	37.990	74.135	71.916

Table 4. Dissipated energy E and maximum equivalent plastic strain ε^{p} at the connection.

Case	$\bar{\varepsilon}^{\mathrm{p}}$	E (kN $\cdot$ mm)	ε^{p}
Case 0	—	47611	0.47342
Case 1	0.047342	46828	0.030721
Case 2	0.0094683	42531	0.0083073

The optimal shapes for Cases 1 and 2 are shown in Figs. 8(a) and (b), respectively. The y-coordinates $y_3, \ldots, y_6$ of the control points 3–6 of the normal and optimal shapes are listed in Table 3. Basically, the optimal shapes share a similar pattern featured with a single concave region, which has two functions: (1) shift the maximum deformation demand from the welded section to a middle section, and (2) increase the plastification area throughout the specified loading history.

The dissipated energy E and the maximum equivalent plastic strain ε^{p} are listed in Table 4 for Cases 0–2. It is seen from this table that the dissipated energy decreases with the decrease of allowable maximum equivalent plastic strain. This is quite reasonable from optimization point of view; i.e., the objective function is smaller for stricter constraints in a maximization problem. It is seen that the dissipated energy of Case 0 is not much different from those of Cases 1 and 2, whereas its maximum equivalent plastic strain is significantly larger than those of Cases 1 and 2. For instance, almost the same (with a difference of about 1.6%) dissipated energy of Case 0 is achieved by the optimal shape for Case 1 with less than 10% of ε^{p}.

Table 5. Dissipated energy E of the normal beam considering the upper bound ε^{p} for the maximum equivalent plastic strain at the fixed end.

	$\bar{\varepsilon}^{\mathrm{p}}$	E (kN · mm)	time
Case 1	0.047342	4714.5	0.72422
Case 2	0.0094683	701.54	0.30078

(a) Case 0

(b) Case 1 $(\bar{\varepsilon}^{\mathrm{p}} = 0.047342)$

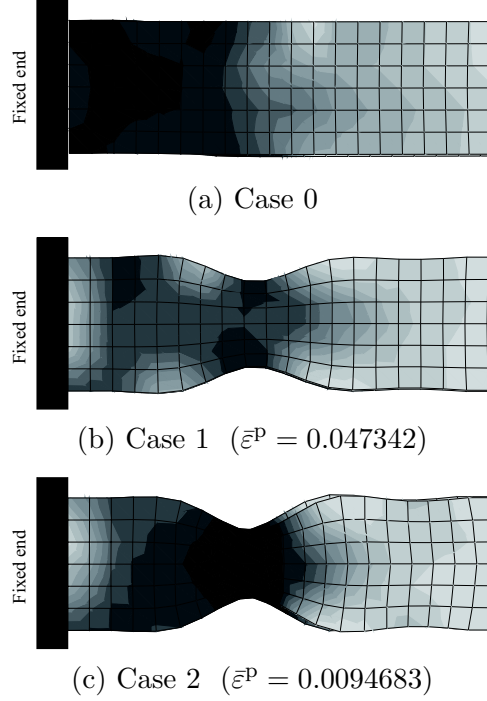(c) Case 2 $(\bar{\varepsilon}^{\mathrm{p}} = 0.0094683)$

Fig. 9. von Mises stress of normal and optimal shapes.

Figs. 9(a)–(c) show the distributions of the von Mises stress for Cases 0–2, respectively, at time $t \simeq 1.875$ corresponding to $\theta = -0.04$. Figs. 10(a)–(c) show the distribution of the equivalent plastic strain at the final state also for Cases 0–2, respectively.

In Figs. 9 and 10, darker color represents larger values. As is seen, the maximum equivalent plastic strain of Case 0 exists at the welded section, whereas it is successfully shifted to the middle section at the concave region for Cases 1 and 2. The distribution of the von Mises stress shows that the lengths of the plastified region of Cases 1 and 2 are larger than that of Case 0. This is particularly because the optimal concave shape allows larger plastified region by realizing a smooth deformed shape against the specified average deflection angle. Owing to the enlarged region, the total plastified areas of Cases 1 and 2 are not much smaller than the area of Case 0, although the concavity decreases the flange width of the plastified region.

It should also be noted from Fig. 8 that the optimal shapes of reduced beam section depend on the value of $\bar{\varepsilon}^{\mathrm{p}}$. Obviously, larger reduction of the flange width is needed for smaller value of $\bar{\varepsilon}^{\mathrm{p}}$ to suppress the deformation at the welded section for the specified history of deflection at the free end. The value of $\bar{\varepsilon}^{\mathrm{p}}$ in practice can be defined by the design criteria along with the concept of the performance-based design.

To further demonstrate the effect of flange shape optimization, the values of E and θ of

(a) Case 0

(b) Case 1 $(\bar{\varepsilon}^{\mathrm{p}} = 0.047342)$
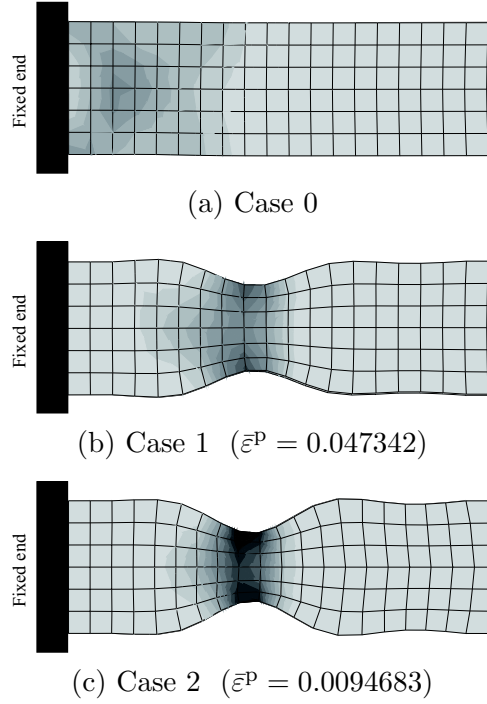
(c) Case 2 $(\bar{\varepsilon}^{\mathrm{p}} = 0.0094683)$

Fig. 10. Equivalent plastic strain of normal and optimal shapes.

the normal beam considering the upper bounds 0.047342 and 0.0094683 for ε^{p} are listed in Table 5, where the time at which constraint is satisfied in equality is also listed. It can be observed by comparing Tables 4 and 5 that the dissipated energy of normal beam is far smaller than that of an optimal beam for the same value of $\bar{\varepsilon}^{\mathrm{p}}$. For $\bar{\varepsilon}^{\mathrm{p}} = 0.0094683$; e.g., the dissipated energy is about 1.5% of the optimal value (Case 2 in Table 4). Hence, the energy dissipation capacity and deformation capacity are significantly increased by optimization.

The reaction forces of the normal and optimal beams are plotted in Fig. 11 with respect to the average deflection angle. It can be confirmed that a smaller $\bar{\varepsilon}^{\mathrm{p}}$ leads to a weaker beam in terms of initial stiffness and strength. However, the initial stiffness and final strength are only slightly reduced by optimization.

The convergence property of the objective function is shown in Fig. 12 for Case 2. As is seen, a large reduction of the objective value is allowed in the initial stage, and the objective value gradually converges to the optimal value. Note that a good approximate solution is found in about 300 analyses. The optimization process is terminated at 3000 analyses, and the elapsed time for optimization is 144 hrs. The average CPU time for one analysis is 170 sec. The time for preprocess, postprocess, ABAQUS license checking, and SA algorithm are very small, and almost all of the elapsed time is used for analysis.

6   Conclusions

Optimal shapes of reduced beam section have been found for a cantilever H-beam subjected to cyclic static forced displacement at the free end of the cantilever beam. The objective function to be maximized is the plastic dissipated energy. The constraint is given
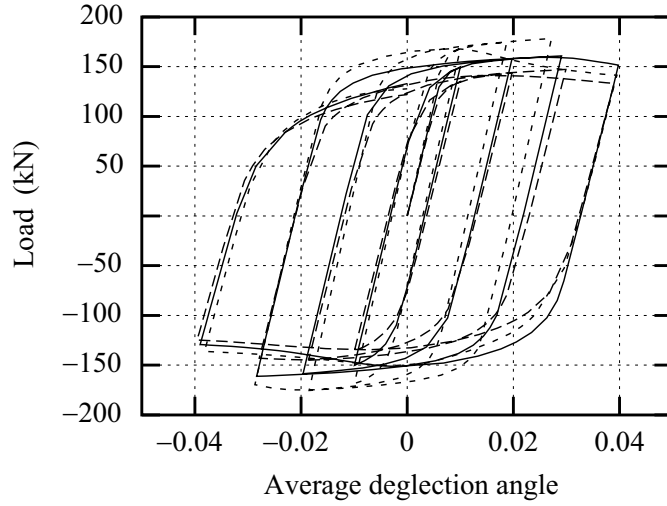
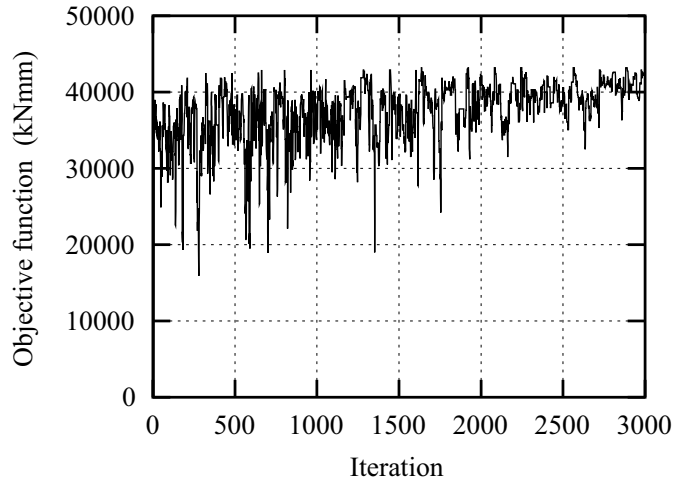Fig. 11. Load-displacement relation. Dotted line Case 0, Solid line: Case 1, Dashed line: Case 2.

Fig. 12. History of objective function by SA for Case 2.

for the maximum equivalent plastic strain at the welded section (fixed end) at the final state.

The accuracy of the numerical results by finite element analysis has been verified in comparison to the experimental results. It has been shown that the optimal shapes can be successfully obtained by SA in conjunction with a commercial finite element analysis code. The optimal shape strongly depends on the upper bound of the equivalent plastic strain, which is to be specified in practice based on the performance required for each frame. The energy dissipation capacity can be significantly improved by optimization compared with the normal beam with uniform flange width.

7 Acknowledgement

References

[1] M. Ohsaki, T. Kinoshita, and P. Pan. Multiobjective heuristic approaches to design of frames with standard sections. *Earthquake Engng. Struct. Dyn.*, 36(11):1481–1495, 2007.

[2] H. A. Eschenauer and N. Olhoff. Topology optimization of continuum structures: A review. *Appl. Mech. Rev.*, 54(4):331–389, 2001.

[3] M. P. Bendsøe and O. Sigmund. *Topology Optimization: Theory, Methods and Applications.* Springer, 2003.

[4] V. V. Bertero, J. C. Anderson, and H. Krawinkler. Performance of steel building structures during the Northridge earthquake. Technical report, Earthquake Engineering Research Center., Univ. of California at Berkeley, Berkeley, CA, 1994.

[5] Recommended seismic design criteria for new steel moment-frame buildings, fema-350. Technical report, Federal Emergency Management Agency, 2000.

[6] A. Plumier. The dogbone: back to the future. *Eng. J.*, 34(2):61–67, 1997.

[7] S. J. Chen, C. H. Yeh, and J. M. Chu. Ductile steel beam-to-column connections for seismic resistance. *J. Struct. Engng., ASCE*, 122(11):1292–1299, 1996.

[8] N. R. Iwankiw and C. Carter. The dogbone: a new idea to chew on. *Modern Steel Constr.*, 36(4):18–23, 1996.

[9] R. Tremblay, N. Tchebotarev, and A. Filiatrault. Seismic performance of RBS connections for steel moment resisting frames: Influence of loading rate and floor slab. In *Proc., Stessa '97, Kyoto*, pages 64–671, 1997.

[10] S. C. Goel, B. Stojadinovic, and K. H. Lee. Truss analogy for steel moment connections. *Eng. J.*, 37(2):43–53, 1997.

[11] E. P. Popov, T. S. Yang, and S. P. Chang. Design of steel MRF connections before and after the 1994 Northridge earthquake. *Eng. Struct.*, 20(12):1030–1038, 1998.

[12] M. D. Engelhardt. The 1999 T. R. Higgins lecture: Design of reduced beam section moment connections. In *Proc., 1999 North American Steel Construction Conf., Tront*, pages 1–29, 1999.

[13] J. Shen, T. Kitjasateanphun, and W. Srivanich. Seismic performance of steel moment frame with reduced beam sections. *Eng. Struct.*, 22:968–983, 2000.

[14] S. K. Kassegne. Development of a closed-form 3-D RBS beam finite element and associated case studies. *Eng. Struct.*, 29:1580–1595, 2007.

[15] M. D. Engelhardt, G. T. Fray, M. Venti S. Jones, and S. Holliday. Behavior and design of radius cut, reduced beam section connections. Technical report, SAC Joint Venture, Sacramento, CA, 2000.

[16] S. L. Jones, G. T. Fry, and M. D. Engelhardt. Experimental evaluation of cyclically loaded reduced beam section moment connections. *J. Struct. Eng.*, 128(4):441–451, 2002.

[17] P. Pan, M. Ohsaki, and H. Tagawa. Shape optimization of H-beam flange for maximum plastic energy dissipation. *J. Struct. Engng., ASCE*, 133(8):1176–1179, 2007.

[18] M. Ohsaki and J. S. Arora. Design sensitivity analysis of elasto-plastic structures. *Int. J. Num. Meth. Engng.*, 37:737–762, 1994.

[19] M. Ohsaki. Sensitivity analysis of elastoplastic structures by using explicit integration method. *Appl. Mech. Rev.*, 50(11):156–161, 1997.

[20] M. Kleiber. *Parameter Sensitivity in Nonlinear Mechanics.* John Wiley & Sons, Chichester, U.K., 1997.

[21] C. C. Swan and I. Kosaka. Voigt–reuss topology optimization for structures with nonlinear material behaviors. *Int. J. Num. Meth. Engng.*, 40:3785–3814, 1997.

[22] C. Reeves. *Modern Heuristic Techniques for Combinatorial Problems.* McGraw-Hill, New York, 1995.

[23] E. Aarts and J. Korst. *Simulated Annealing and Boltzmann Machines: A Stochastic Approach to Combinatorial Optimization and Neural Computing.* Wiley, Chichester, U. K., 1989.

[24] R. J. Balling. Optimal steel frame design by simulated annealing. *J. Struct. Engng., ASCE*, 117(6):1780–1795, 1991.

[25] H. Tagawa and M. Ohsaki. A continuous topology transition model for shape optimization of plane trusses with uniform cross-sectional area. In *Proc. 3rd World Congress of Structural and Multidisciplinary Optimization (WCSMO3)*, 1999.

[26] V. Braibant and C. Fleury. Shape optimal design using B-splines. *Comp. Meth. Appl. Mech. Engng.*, 44:247–267, 1984.

[27] G. Farin. *Curves and Surfaces for Computer Aided Geometric Design.* Academic Press, New York, 1992.

[28] M. Ohsaki and M. Hayashi. Fairness metrics for shape optimization of ribbed shells. *J. Int. Assoc. Shells and Spatial Struct.*, 41(1):31–39, 2000.

[29] *ABAQUS Version 6.4 Documentation.* ABAQUS, Inc., 2004.

[30] W. L. Goffe, G. D. Ferrier, and J. Rogers. Global optimization of statistical functions with simulated annealing. *J. Econometrics*, 60(1):65–99, 1994.

[31] B. David. *Python Essential Reference (2nd Edition).* New Riders Publishing, 2001.

Appendix

The procedure for connecting ABAQUS and the SA program is described below.

As shown in Fig. 13, the SA program generates new coordinates of the control points, which are the design variables of the optimization problem. This information is transmitted to ABAQUS preprocessing module that creates the beam model. The entire preprocessing module is controlled by a Python script language [31] that serves as the programming interface of ABAQUS. The control script consists of the following six steps:
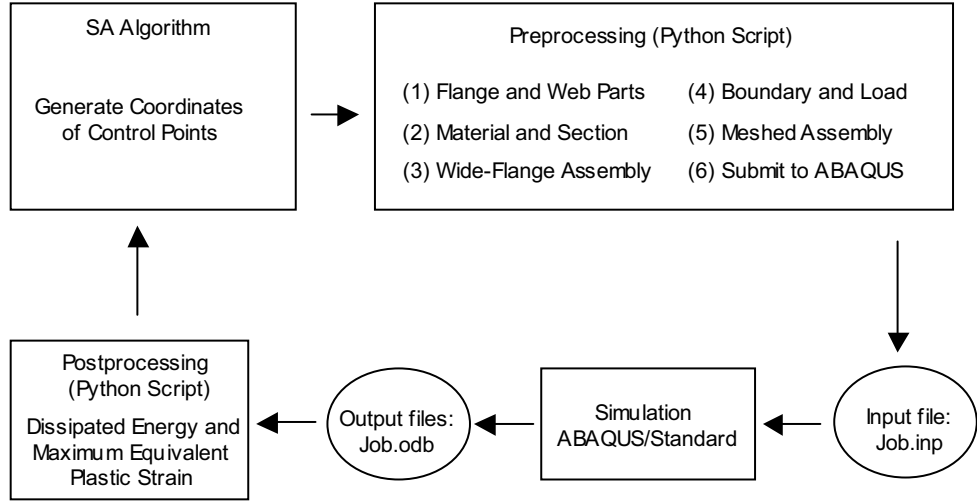
Fig. 13. Flowchart of ABAQUS analysis.

(1) Two parts, i.e., a flange part and a web part, are created. The cutout shape of the flange is determined using a cubic spline curve in reference to the control points.
(2) Materials and section geometries are defined, and assigned to respective parts.
(3) Two instances of the flange part, which represents the upper and lower flanges, and a instance of the web part are imported to form an assembly. The assembly is further merged to a single beam assembly.
(4) Boundary and loading conditions are defined for the analysis.
(5) The beam assembly is discretized to S4R quadrilateral shell elements.
(6) An analysis job is submitted to ABAQUS.

In the analysis, ABAQUS/Standard is used for solving the problem defined in the '.inp' file created by ABAQUS preprocessing module. An '.odb' file, which contains the analysis results, is generated. A postprocessing module also written by the Python script language is used to extract the necessary data such as the dissipated energy and the maximum equivalent plastic strain near the beam-column connection from the '.odb' file. The data are returned to the SA program for the new round of iteration.